A Model Predictive Control for a Four-Zone Medium-Voltage AC/DC Electric Ship

Joseph Young
OptimoJoe
Houston, TX
Email: joe@optimojoe.com

David G. Wilson
Electrical Science
Sandia National Laboratories
Albuquerque, NM
Email: dwilso@sandia.gov

Marvin A. Cook
Systems Research, Analysis, and Applications
Sandia National Laboratories
Albuquerque, NM
Email: macook@sandia.gov

Wayne Weaver
Mechanical Engineering
Michigan Technological University
Houghton, MI
Email: wwweaver@mtu.edu

Steven Glover
Electrical Science
Sandia National Laboratories
Albuquerque, NM
Email: sfglove@sandia.gov

***Abstract*—The following paper provides details of a model predictive control designed to operate a four-zone medium-voltage AC/DC electric ship. The control incorporates a reduced order model (ROM) that describes the ship components, a discretization of the dynamics produced by the ROM, and an optimization formulation that determines the ship's behavior. This includes details on how to effectively abstract the power system components into a form that integrates well with computational optimizers. Then, the control is validated on a operational vignette based on mission profiles.**

I. Introduction

In the past several years, there has been an increased emphasis on the design of electric ships for the navy. These ships possess a variety of unique challenges such as the need for large amounts of power for pulsed mission loads which may require response times faster than what the prime generation can provide [1]. Mission pulsed loads that support the next generation of navy ships will impact the integrated power and energy system architecture. It is projected that an increased demand for evolved power conversion systems coupled with energy storage systems is required to meet peak power demand [2]. A big driver is that during the pulsing cycle, of these numerous mission pulsed loads, sufficient energy storage will be required to efficiently operate repetitively. The key to managing all this power is an *energy magazine* that employs state-of-the-art energy storage systems and advanced controls for energy and power management [2].

Integration of multiple energy sources and storage systems into new and evolving ship power systems requires an efficient power management system and many recent developments of control technologies and power management strategies have been proposed for conventional AC ship power systems [3]. Although, to support the navy ship peak power demand scenarios a more advanced control and power management solution will be necessary. Ren et al. have investigated a multi-energy integrated ship energy management system that is based on a hierarchical control collaborative optimization strategy [4]. The hierarchical control technique demonstrates a reduction in power losses with an efficient optimization approach among other benefits. Nguyen et al. has investigated an original energy management methodology for enhancing the resilience of ship power systems [5]. There, they consider multiple types of energy storage systems that are based on battery and supercapacitor implementations. The primary function of this proposed energy management system is to maximize the load operability while taking ramp-rate characteristics of energy storage systems and generators into account. Simulation results have demonstrated the effectiveness of the method in managing the energy storage systems, which ensure the systems resilience under generation power shortages. In addition, the energy storage ramp rates are an important parameter for navy ship applications. Recently, Rigatos et al. consider simple and computationally efficient solutions for the nonlinear optimal control problem of shipboard AC/DC hybrid microgrid power systems [6]. This includes a stabilizing optimal (H-infinity) feedback controller design. Many of these elements discussed in the above publications are necessary considerations for the next generation navy ship power systems.

In order to study and control these systems, there has been development of four-zone notional systems for both Medium Voltage DC (MVDC) [7] and Medium Voltage AC (MVAC) [8] systems. In particular, Greene et al. [8] developed a ROM well-suited for the study of a hybrid MVAC/MVDC electric ship and its associated Energy Storage System (ESS). Simultaneously, Young et al. developed a model predictive control to optimize the performance of a ship based on a similar ROM in [9]. The purpose of this paper is to extend that work to the more detailed ROM found in [8]. This includes re-abstracting the power system components into a form well-suited for computational optimization.

In pursuit of this goal, this paper presents a model predictive control (MPC) designed to operate an electric ship. Also called an on-line optimal control, this control is formed by solving an optimization formulation based on a reduced-order model of the ship over a finite-time horizon. This model must necessarily include a prediction of any anticipated loads or generation capacity. Once a solution to this formulation is found, the resulting control is used for as long as the model accurately represents the state of the ship. Then, the process repeats. Therefore, an MPC represents a type of feedforward control, but one that can be combined with a feedback control to enhance performance. The behavior of the control is determined by the ROM used, the performance metrics integrated into the objective, bounds enforced on the control or state, and the prediction of the transient elements within the system.

Once the MPC has been formulated as an optimization problem, further decisions must be made as to how to integrate it into a computational optimization solver, which also affects the behavior of the control. This includes the process of discretiza-

tion. In this context, discretization means the transformation of the ordinary differential equations (ODEs) or differential algebraic equations (DAEs) that represent the dynamics into a computable linear system. In general, there are two approaches to discretizing an optimization formulation. Either the optimization formulation is discretized directly in a process called discretize-then-optimize or the first-order optimality conditions are discretized in a process called optimize-then-discretize. The process of discretize-then-optimize is also known as direct transcription and this approach is described in greater detail by authors such as Betts [10]. This paper employs a discretize-then-optimize approach due to the ease of integration with a nonlinear optimization algorithm. In a optimize-then-discretize approach, care must be paid to the inner product used in the discretization or else the discretized derivatives may not be accurate to machine precision.

Next, the dynamics may be discretized using a variety of methods such as a Runge-Kutta method, which discretizes the dynamics in time, or a collocation method, which discretizes the dynamics in the function space.

This paper discretizes the dynamics using an orthogonal spline collocation (OSC) method, which is also known as a pseudospectral method. In an OSC method, the state and control variables are discretized in the function space, akin to a finite element method, rather than in time such as with Tustin's method or a trapezoidal rule. Then, the dynamics are satisfied at a set of collocation points, which are chosen to be the roots of a collection of mutually orthogonal polynomials. Generally, these are the same set of points used in quadrature algorithms. This process is more carefully described by authors such as de Boor and Swartz [11] who used Gaussian quadrature points. The combination of collocation and direct transcription has also been explored in Pietz's thesis [12]. This algorithm discretizes the state and control variables using Bernstein polynomials and then satisfies the dynamics at Gaussian quadrature points or Chebyshev points. This approach was first described by Young, Wilson, Weaver, and Robinett in [13] and later used by Young et al. in [14], [9], [15], [16]. This algorithm in this paper differs from those works in that it disconnects the Bernstein polynomial based spline in a manner that results in better behaved linear systems. This is the same process used in [17], but that algorithm uses Guass-Lobatto points in lieu of Chebyshev points for increased accuracy. In each of these cases, the algorithm produces a continuous-time control. If a discrete time control is desired, the control can be sampled at discrete points.

The choice to use Bernstein polynomials in this paper is intentional and has a variety of benefits useful for optimal control. Specifically, since the evaluation of a Bernstein polynomial is a convex combination of its coefficients [18], bounding the coefficients of the polynomial between l and u will in turn bound the polynomial itself between l and u. This bound holds over the entire domain and not just at the mesh or collocation points. In addition, since the derivative of a Bernstein polynomial is another Bernstein polynomial, higher-order derivatives can be similarly bounded. In other words, a Bernstein polynomial based spline, and its derivatives, can be bounded using linear inequality constraints. In order to model nonlinear bounds, the difference between a Bernstein polynomial and a second constant Bernstein polynomial can be bounded. Practically, these enable limits to be placed on the power system components themselves, such as the overall energy stored in an energy storage device, or its dynamics such as a limit to the ramp rate of how quickly a storage device can charge or discharge.

The combination of Bernstein polynomials with an OSC method also has the benefit that the time-scales for the state and control are separated. Generally speaking, the state of the system reacts to both the external inputs as well as the controls themselves. If the control operates as fast as the state, the discretization of the state may not possess enough fidelity to accurately represent the transients that result from these rapid changes made by the control. This affect can be mitigated by forcing the control to operate on a slower time scale than the state. An auxiliary benefit of this separation is that the accuracy of the state solves can be improved through adaptive mesh refinement independent of the control.

Due to their efficacy, a variety of other similar control algorithms exist commercially. For example, MathWorks offers the Model Predictive Control Toolbox [19]. The algorithm within this paper differs from this toolbox in the discretization. The MPC Toolbox discretizes its nonlinear MPC in time using an implicit trapezoidal rule, known also as Tustin's method. This produces a discrete time control where the state and control variables operate at the same time fidelity. As a result, the bounds on these variables are only enforced at the sample points. As an alternative, GPOPS-II [20] implements a continuous time MPC based on a collocation method. This approach is similar to this paper in that they both produce a continuous time control, utilize a collocation method, and support adaptive mesh refinement. They differ in the kinds of polynomials used within the discretization as well as the location of the collocation points. As a result, the bounds in GPOPS-II are only enforced at the collocation points rather than over the entire domain.

The contribution of this paper is multi-fold. This paper improves upon the results in [9] in that it uses a more accurate, faster converging algorithm. It does so by improving the discretization to remove modeling redundancies as well as better isolating the control elements in the MVAC system. In addition, the ROM of the electric ship has been improved to include a combination of MVDC, MVAC, and spinning machine elements. This matches the model used by Greene et al. in [8].

In order to validate this approach, this algorithm is applied to an operational vignette based the propulsion and mission load profile from [8], which was extracted from [21]. The results can be found below.

II. Model

This paper models the microgrid of an electric ship as a four zone system consisting of four Main Turbine Generators (MTGs), four Propulsion Motor Modules (PMMs), eight Energy Magazines (EMs), and four Mission Loads (MLs). These are interconnected by a combination of MVAC and MVDC buses and the overall topology can be seen in fig. 3. In total, this topology includes 136 power system components and connections. The components and topology for the ROM are based on those from [8], which uses the inverter model from [22].

In order to model these elements, five different kinds of power system components and five different kinds of connections are required. These components are described by the circuits in figs. 1 and 2. First, figs. 1a and 1b can represent either a bus that receives and delivers power to other components or acts as a device that coordinates various mission loads. The difference between them is that fig. 1a represents a DC bus whereas fig. 1b represents a 3-phase AC bus transformed into the dq0 reference frame. Required mission loads are represented as the controlled source i_p and dispatchable mission loads are

represented as the controlled source i_d. As for energy storage, u models an energy storage device connected to the bus. Its maximum amount of storage, charge, and discharge rates are modeled and bounded separately. Second, figs. 1c and 1d models the connection between two different parallel buses or a connection between a spinning machine and a parallel bus. The difference between them is that fig. 1c represents a DC power component whereas fig. 1d represents a three-phase AC component transformed into the dq0 reference frame. In addition to modeling connections between different grid buses, these components can be used to model inverter based generation by setting a constant voltage source and bounding the amount of current allowed out of component. Though, this capability is not used in the current ship model.

Sitting between the components a variety of connections. First, fig. 2a represents an ideal transformer. Here, power is preserved, but the ratio between current and voltage can vary. Second, fig. 2b represents an ideal gyrator. Like the transformer, power is preserved, but the voltage drop is dictated by the current and ratio. Generally, this component is used to couple a series spinning machine to a series DC or 3-phase AC component. Next, fig. 2c models an ideal transformer with multiple connections. Power is preserved, but the outgoing current is divided according to a convex combination. Finally, fig. 2e and fig. 2d represent a power converter from DC to 3-phase AC and 3-phase AC to DC.

Each variable may contain an initial condition, bound, or a multiplicative linkage. Further, each of these additional conditions may be placed on the variable itself or on its derivative. Generally speaking, these conditions are used to add additional model information to the dynamics that are not explicitly made available in the circuit-based ROM. For example, in order to limit the maximum amount of energy stored in an energy storage device, the bound $0 \leq w \leq w_{max}$ can be added. In order to set the initial amount of energy storage, the initial condition $w(0) = w_0$ can be used. Finally, in order to coordinate two different energy storage devices, so that one does not charge another, two constraints can be multiplied and bounded such as $u = u_1 u_2$ and $u \geq 0$. This ensures that the variables share the same sign.

The dynamics for these models can be found in the following set of equations. In short, the microgrid is represented as a DAE subject to a variety of bounds that constrain the behavior of the system.

Parallel DC bus	$Cv' + \frac{v}{R} + \sum i_p + \sum i_d + \sum i_{snk} = \sum i_{src} + u$
Parallel DC energy storage	$w' = -vu$
	$w \geq 0$
Parallel DC non-dispatchable load	$i_p = \frac{P}{v}$
Parallel DC dispatchable load	$i_d = \frac{d}{v}$
Parallel 3-phase AC bus	$Cv'_d + \frac{v_d}{R} - \omega C v_q + \sum i_{p_d} + \sum i_{d_d} + \sum i_{snk_d} = \sum i_{src_d} + u_d$
	$Cv'_q + \frac{v_q}{R} + \omega C v_d + \sum i_{p_q} + \sum i_{d_q} + \sum i_{snk_q} = \sum i_{src_q} + u_q$
Parallel 3-phase AC energy storage	$u_d = \sqrt{\frac{3}{2}} u_m \cos(\theta_u)$
	$u_q = \sqrt{\frac{3}{2}} u_m \sin(\theta_u)$
	$w' = -v_d u_d - v_q u_q$
	$w \geq 0$
Parallel 3-phase AC non-dispatchable load	$i_{p_d} = \frac{P\cos(\theta_p)}{\cos(\theta_p)v_d + \sin(\theta_p)v_q}$
	$i_{p_q} = \frac{P\sin(\theta_p)}{\cos(\theta_p)v_d + \sin(\theta_p)v_q}$
Parallel 3-phase AC dispatchable load	$i_{d_d} = \frac{d\cos(\theta_d)}{\cos(\theta_d)v_d + \sin(\theta_d)v_q}$
	$i_{d_q} = \frac{d\sin(\theta_d)}{\cos(\theta_d)v_d + \sin(\theta_d)v_q}$
Series DC bus	$Li' + Ri + v_{snk} = v_{src} + u$
Series DC energy storage	$w' = -ui$
	$w \geq 0$
Series 3-phase AC bus	$Li'_d + Ri_d - \omega L i_q + v_{snk_d} = v_{src_d} + u$
	$Li'_q + Ri_q + \omega L i_d + v_{snk_q} = v_{src_q} + u$
Series 3-phase AC energy storage	$u_d = \sqrt{\frac{3}{2}} u_m \cos(\theta_u)$
	$u_q = \sqrt{\frac{3}{2}} u_m \sin(\theta_u)$
	$w' = -u_d i_d - u_q i_q$
	$w \geq 0$
Series spinning machine	$J\omega' + B\omega + \tau_{snk} = \tau_{src} + u$
Series spinning machine storage	$w' = -u\omega$
	$w \geq 0$
Transformer	$v_{src} = K\lambda v_{snk}$
	$i_{snk} = K\lambda i_{src}$
	$\lambda \geq 0$
Gyrator	$v_{src} = K\lambda i_{snk}$
	$v_{snk} = K\lambda i_{src}$
	$\sum_{k=1}^{m} \lambda_k = 1$
	$\lambda_k \geq 0$
Selector	$v_{src} = K \sum_{k=1}^{m} \lambda_k v_{snk_k}$
	$i_{snk_k} = K\lambda_k i_{src}$
	$\lambda_k \geq 0$
3-phase AC to DC converter	$v_{src_d} = \sqrt{\frac{3}{2}} \cos(\theta) v_{snk}$
	$v_{src_q} = \sqrt{\frac{3}{2}} \sin(\theta) v_{snk}$
	$i_{snk} = \sqrt{\frac{3}{2}} (\cos(\theta) i_{src_d} + \sin(\theta) i_{src_q})$
DC to 3-phase AC converter	$v_{src} = \sqrt{\frac{3}{2}} (\cos(\theta) v_{snk_d} + \sin(\theta) v_{snk_q})$
	$i_{src_d} = \sqrt{\frac{3}{2}} \cos(\theta) i_{src}$
	$i_{src_q} = \sqrt{\frac{3}{2}} \sin(\theta) i_{src}$
Initial condition	$v^{(k)}(0) = v_{k_0}$
General bound	$v_{k_{\min}} \leq v^{(k)} \leq v_{k_{\max}}$
Multiplicative linkage	$v = (v_1^{(k)} - c_1)(v_2^{(k)} - c_2)$

In order to shape the behavior of the control, these dynamics are combined with the following objective functions, which are further weighted and summed together

Least Squares (LS)	$c\|v - v_{trg}\|^2$
Approximate Root Mean Squared (RMS)	$\sqrt{\gamma^2 + c\|v - v_{trg}\|^2} - \gamma$
Integral	$c \int_0^T (v - v_{trg})$

where T denotes the size of the time horizon. Note, approximate RMS objective function provides a continuously differentiable objective that behaves like least-squares for values below γ and RMS for values greater than γ. Also note, each of these objectives are generic and can be applied to any state or control variable as well as their derivatives. Some examples of useful objective functions are

Keep storage device full	$\sqrt{\gamma^2 + \|w - w_{full}\|^2} - \gamma$
Penalize ramp rate in energy storage use	$\sqrt{\gamma^2 + \|w''\|^2} - \gamma$
Track a dispatchable load profile	$\sqrt{\gamma^2 + \|d - d_{trg}\|^2} - \gamma$
Penalize parasitic losses	$R\|i\|^2$
Penalize ringing of voltage on a parallel DC bus	$\sqrt{\gamma^2 + \|v''\|^2} - \gamma$
Force maximum draw to a parallel DC bus	$-\int_0^T i_{snk}$

Combining the dynamics and objective functions above results in the following optimization formulation for the model predictive control

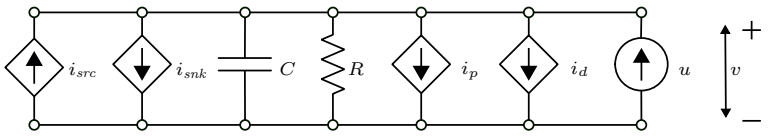

(a) DCP: DC parallel component

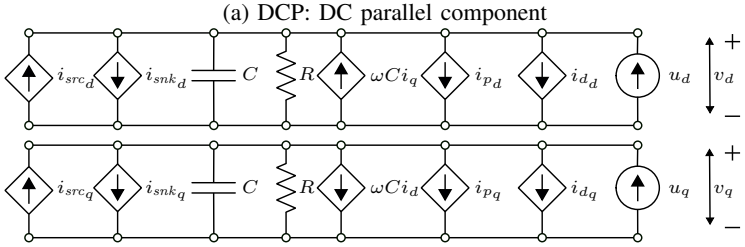

(b) 3ACP: 3-phase AC parallel component

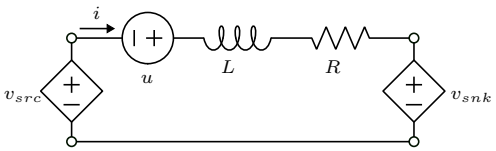

(c) DCS: DC series component

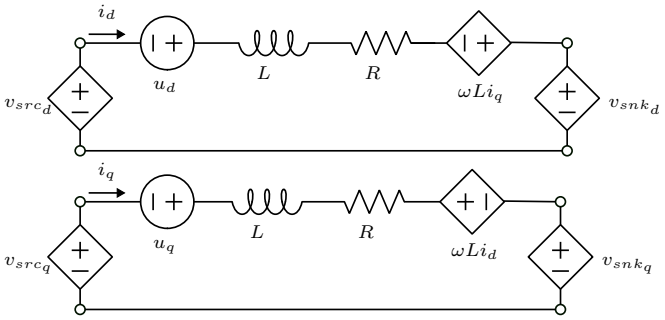

(d) 3ACS: 3-phase AC series component

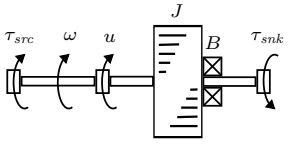

(e) SS: Series spinning machine component

Fig. 1: Grid components that are connected together using the connections in fig. 2 to form a grid.

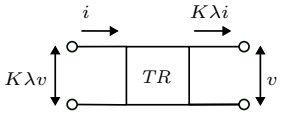

(a) TR: Ideal transformer

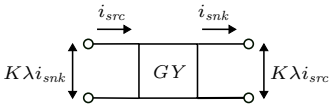

(b) GY: Gyrator

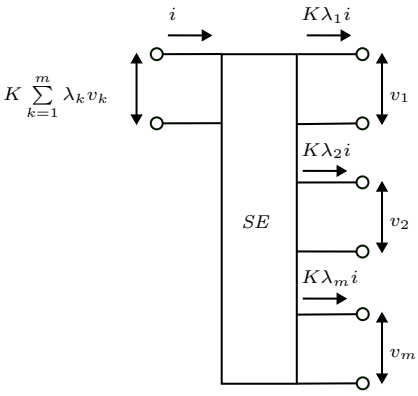

(c) SE: Selector

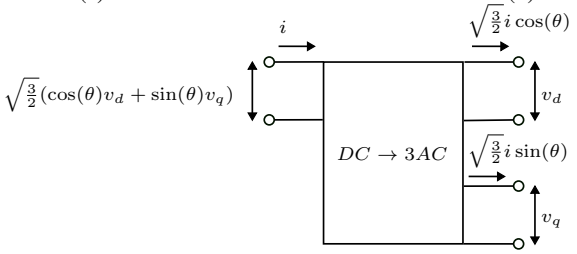

(d) DC/3AC: DC to 3-phase AC converter

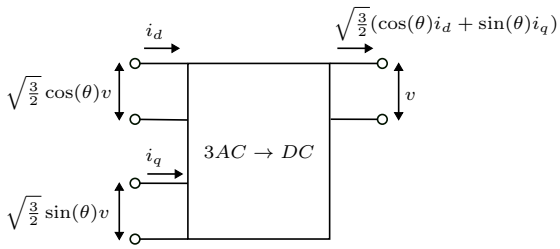

(e) 3AC/DAC: 3-phase AC to DC converter

Fig. 2: These elements connect the grid components in fig. 1 and each conserves power across the connection. Generally, the gyrator is used to connect two series components such as a spinning machine to a 3-phase series component where K represents the machine torque constant.

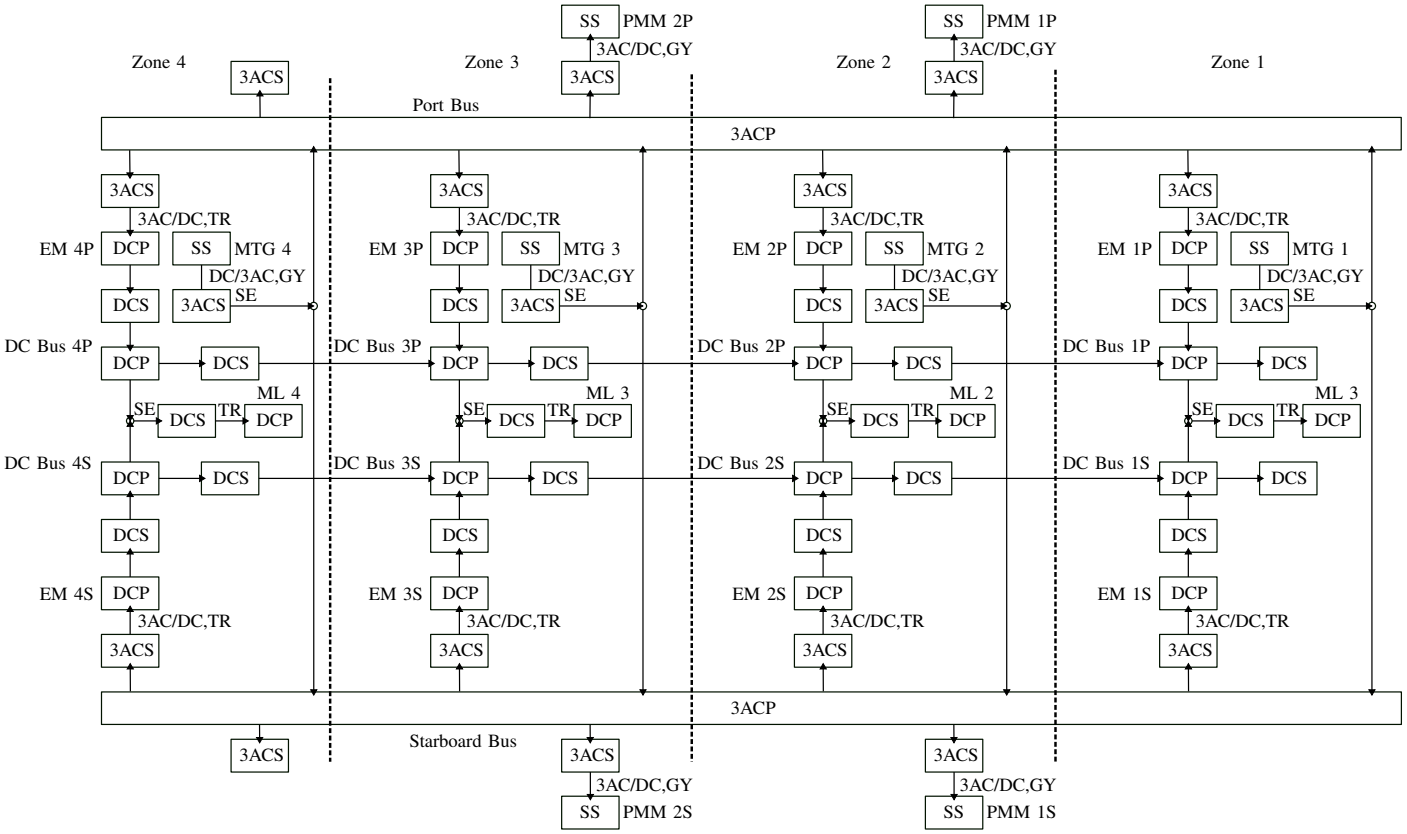

Fig. 3: Reduced order model of a four-zone MVAC/MVDC Navy ship. Each of these components and connections can be found in figs. 1 and 2.

Minimize	Error in desired performance
Subject to	Parallel DC component dynamics
	Parallel AC component dynamics
	Series DC component dynamics
	Series AC component dynamics
	Series Spinning Machine component dynamics
	Bounds on behavior

III. Discretization

As described by the introduction, this algorithm uses an OSC method to discretize the optimal control. In order to implement this approach, the state and control variables are each represented as a spline comprised of Bernstein polynomials, which are then satisfied at a set of collocation points mapped to the divisions in the spline. As a result, if the spline of degree $order$ contains $nele = nmesh - 1$ divisions, then the coefficients that represent the spline can be represented as a vector $c \in \mathbb{R}^{nele \cdot (order+1)}$. Therefore, each state equation requires $nele \cdot (order + 1)$ conditions in order to generate a square invertible system. These conditions are split between those required for the ODE, the smoothness, and the boundary conditions.

As a result, the map between the coefficients and the d-th derivative of the spline evaluated at the collocation points can be represented as a linear operator

$$D^{(d)} \in \begin{cases} \mathbb{R}^{(order+1-smooth)nele+1 \times (order+1)nele}, \\ \quad smooth \text{ is odd} \\ \mathbb{R}^{(order+1-smooth)nele \times (order+1)nele}, \\ \quad smooth \text{ is even} \end{cases}$$

Here, $d \leq \max\{0, smooth - 1\}$ and $smooth$ denotes that the function is $smooth - 1$ times continuously differentiable. In other words, $smooth = 1$ gives a continuous function and $smooth = 2$ gives a continuously differentiable function. This operator is generated by evaluating the dth derivative of the Bernstein polynomial based spline at the Chebyshev points when $smooth$ is odd and the Gaussian quadrature points when $smooth$ is even. Note, there is one additional collocation point when $smooth$ is odd and Chebyshev points are used.

In order to guarantee continuity or smoothness between the elements, the jump in derivative is constrained to zero. In this context, jump means the difference between the derivatives of successive spline polynomials evaluated at the interior mesh points. This gives a set of linear constraints and a jump operator of order $smooth$ can be represented by the operator $J^{(smooth)} \in \mathbb{R}^{(nmesh-2)smooth \times (order+1) \cdot nele}$.

As for the boundary conditions, these are imposed directly on the spline using a process similar to that of the derivative operators. The maximum number of boundary conditions allowed is $(smooth - 1)/2$ initial and terminal conditions, each, when $smooth$ is odd and $smooth/2$ when $smooth$ is even. If fewer boundary conditions are desired, additional collocation points must be added to impose the same number of constraints as variables. This results in an operator

$$B^{(smooth)} \in \begin{cases} \mathbb{R}^{smooth-1 \times (order+1)nele}, \\ \quad smooth \text{ is odd} \\ \mathbb{R}^{smooth \times (order+1)nele}, \\ \quad smooth \text{ is even} \end{cases}$$

The reason this algorithm maintains a switching between the Gaussian quadrature points and Chebyshev points based on the smoothness is to create a set of conditions that impose $order + 1$ constraints on each element equally. This produces a linear system with a lower condition number. The jump operator creates an additional $smooth$ constraints on the interior elements, but only $smooth/2$ constraints on the boundary elements. This occurs because the jump is shared between neighboring elements and the boundary elements have only a

single neighbor. Hence, when $smooth$ is odd, the algorithm is left with half a constraint on the boundary elements. To balance this, Gauss-Lobatto points share their first and last collocation with the neighboring element. As a result, an extra half condition can be gained by using Gauss-Lobatto points when $smooth$ is odd. Then, additional boundary conditions are used to add the remaining constraints.

As an example, a first-order RL circuit governed by the equation

$$\begin{aligned} &Li'(t) + Ri(t) = v(t), \\ &i(0) = i_0 \end{aligned} \tag{1}$$

can be discretized as

$$\begin{bmatrix} LD^{(1)} + RD^{(0)} \\ J^{(2)} \\ [1, 0, \ldots, 0] \end{bmatrix} c = \begin{bmatrix} i(t_{coll}) \\ 0 \\ i_0 \end{bmatrix} \tag{2}$$

where t_{coll} are the collocation points and c are the coefficients of the spline. Note, one additional collocation point is required in the final element to balance the initial condition and this is included implicitly above.

The discretization can be further improved by using both domain and codomain transforms. In a codomain transform, the discretized dynamics are scaled by $\text{Diag}(\sqrt{w})$ where w are the Gauss-Lobatto integration weights when $smooth$ is odd or the Gaussian quadrature weights when $smooth$ is even. This alters the formulation so that the ℓ^2-norm of the error in the discretized dynamics corresponds to the L^2-norm in the continuous formulation. Similarly, in the domain transform, the optimization variables are scaled by $(\text{Diag}(\sqrt{w})D^{(0)})^{-1}$. Here, the scaling has an inverse since it transforms from a scaled collocation space back to the space of coefficients. In this way, the ℓ^2-norm of the discretized state and control variables corresponds to the L^2-norm of their functional counterpart. In practical terms, the domain and codomain transforms are important because they allow the state and control variables to be refined either in the size of the elements, h, or in the polynomial order, p, where the norm of the residuals or the variables themselves do not change. This means that the optimization algorithm does not need to be reparameterized during refinement. For example, the initial size of the trust-region radius does not need to be adjusted.

IV. Computational Study

The following operational vignette is based the propulsion and mission load profile from [8], which was extracted from [21]. These profiles can be found in the plots below.

For the objective, there are two types split between 12 components. First, the mission load on the ML components is considered a dispatchable, so the control attempts to follow the mission load profile as closely as possible. Second, explicit energy storage devices exist on the EMs, so the control attempts to keep them at 95% full, but this is prioritized lower than supplying power to the dispatchable loads. The number 95% is used to give the energy storage system some leeway in keeping the system stable by allowing it to store or deliver power as needed

In terms of the discretization, the state variables use a high-order discretization on a fine mesh whereas the control variables use a cubic discretization on a coarser mesh. The reason for this difference is to limit the complexity of the control in order to force a control scheme that is easier to implement in machinery. This is a design choice and not a limitation of the algorithm.

The rest of the parameters that characterize the model are summarized in the table below.

MTG torque , τ_{src}	Variable $\mathrm{N\,m}$
MTG friction. , B	1×10^{-6} N
MTG mass moment., J	$100\ \mathrm{kg\,m^2}$
MTG freq., ω	$\omega \in [9900, 10\,100]$ RPM, $10\,000$ RPM $\pm$ 1%
PMM torque , τ_{src}	Specified (see plot)
PMM friction. , B	1×10^{-6} N
PMM mass moment., J	$100\ \mathrm{kg\,m^2}$
PMM freq., ω	$\omega \in [9900, 10\,100]$ RPM, $10\,000$ RPM $\pm$ 1%
Port/Star. voltage, v	$v \in [12\,870, 13\,130]$ V, $13\,000$ V $\pm$ 1%
Port/Star. resist., R	5000 Ω
Port/Star capac., C	0.001 F
DC bus voltage, v	$v \in [9900, 10\,100]$ V, $10\,000$ V $\pm$ 1%
DC bus resist., R	100 Ω
DC bus capac., C	0.01 F
EM voltage, v	$v \in [9900, 10\,100]$ V, $10\,000$ V $\pm$ 1%
EM resist., R	500 Ω
EM capac., C	0.01 F
EM energy stor., w	$w \in [0, 1 \times 10^6]$ J
EM energy stor. objective	Keep 95% full
ML voltage, v	$v \in [9900, 10\,100]$ V, $10\,000$ V $\pm$ 1%
ML resist., R	100 Ω
ML capac., C	0.01 F
ML disp. load, D	Specified (see plot)
ML disp. objective	Match mission load
3-phase AC series conn freq., ω	$\omega \in [9900, 10\,100]$ RPM, $10\,000$ RPM $\pm$ 1%
3-phase AC series conn. induct., L	1×10^{-6} H,
3-phase AC series conn. resist., R	1×10^{-6} Ω
DC series conn. induct., L	1×10^{-3} H,
DC series conn. resist., R	1×10^{-2} Ω
State var. disc. order	12
State var. disc. mesh	24 elements
Control var. disc. order	3
Control var. disc. mesh	49 elements

The resulting optimization formulation is solved using a prototype version of Optizelle [23]. This algorithm implements a modified version of the composite step SQP method developed by Ridzal and Heinkenschloss [24], [25], [26] combined with a primal-dual interior point method in a manner similar to NITRO described by Byrd, Hribar, and Nocedal [27]. The linear systems produced by this formulation are solved using a rank-revealing QR factorization developed by Davis [28]. Overall, the formulation contains 78846 variables, 40160 equations, and 35472 bounds.

The overall behavior of the control can be seen in fig. 4. The specified torque to the PMMs can be seen in fig. 4a. The optimal control specifies a limit to the variation in the frequency of the motor and accomplishes this with a deviation of less than 0.1%. Next, the behavior of the MTG's torque control can be seen in fig. 4b. Recall, the torque is a control input chosen to not only produce sufficient power for the grid, but to maintain the appropriate frequency. The control does so with less than 0.1% deviation in the desired frequency, which can be seen in fig. 4c. Next, consider the voltage on a variety of buses in fig. 4d. Here, it can be seen that the desired voltage also fluctuates less than 0.1% from the desired. Part of how this is moderated is through the use of the transformers. A selection of the phase chosen by the control can be seen in fig. 4e. Note, the phases for each of the power converters virtually align. Finally, fig. 4f shows the amount of desired and delivered power to the mission loads. Outside of some minor ringing due to step inputs from the desired mission loads, the control algorithm delivers the requested amount of power.

Outside of these specific results, the computational study provides the following information. First, the control performs

well. Each of the performance metrics is met and the behavior is well bounded over the entire domain. This helps confirm the efficacy of the OSC method combined with Bernstein polynomials presented in section III. Second, this study confirms that the reduced-order model presented by Greene et al. [8] integrates well with a model predicted control. This process is made simpler when the power system components are abstracted as they are in section II. Finally, these results confirm that a model of an electric ship represented a four zone system consisting of 136 power system components remains computationally in scope for a model predictive control when combined with modern algorithms.

V. Summary and Future Work

The preceding paper provided a high level overview of an optimal control algorithm designed to safely and efficiently operate a electrical grid that models a hybrid MVDC, MVAC, and spinning machine model of an electric ship. While this environment provides some unique challenges such as propulsion loads or rapidly changing mission loads, the control can effectively accommodate these difficulties.

The above control methodology is well-suited for a variety of use cases. For example, when integrated with a feedback control, the optimal control can provide set points for the feedback controller to follow in order to guide the ship through a series of maneuvers and mission loads. Alternatively, the optimal control can assist in the design of the overall grid. For example, the above computational study can provide performance specifications for the amount of energy storage required and suggest the rate at which power should be charged or discharged.

In terms of performance, the control performed well on a sample operational vignette. Both the performance metrics for providing power to a mission load and minimizing the use of energy storage were met. System requirements such as maintaining a certain machine frequency or bus voltage were also met with less than 0.1% deviation.

In terms of future work, additional vignettes, parameterizations, and ship topologies should be investigated. In addition, further improvements to the optimal control algorithm should be incorporated.

Acknowledgment

This work was supported by ONR Future Naval Capabilities for a project entitled Nonlinear Power Flow Control Design for Robust Combat Power Control. In addition, the authors would like to thank our Sponsors; Nathan Spivey and Joseph Borraccini, Program Managers along with their team for their support. This document approved as DISTRIBUTION STATEMENT A. Approved for public release: distribution unlimited.

Sandia National Laboratories is a multi-mission laboratory managed and operated by National Technology and Engineering Solutions of Sandia, LLC., a wholly owned subsidiary of Honeywell International, Inc., for the U.S. Department of Energy's National Nuclear Security Administration under contract DE-NA0003525. The views expressed in the article do not necessarily represent the views of the U.S. Department of Energy or the United States Government.

References

[1] N. Doerry, "Next generation integrated power system ngips technology development roadmap," NAVSEA, Tech. Rep. Ser 05D/349, 2007.

[2] Breaking Defense, "Energy Magazine Gives the Navy Power for Shipboard Lasers and Other High-Energy Systems," *Leonardo DRS*. [Online]. Available: https://www.leonardodrs.com/news/in-the-news/energy-magazine-gives-the-navy-power-for-shipboard-lasers-and-other-high-energy-systems/

[3] M. D. A. Al-Falahi, T. Tarasiuk, S. G. Jayasinghe, Z. Jin, H. Enshaei, and J. M. Guerrero, "Ac ship microgrids: Control and power management optimization," *Energies*, vol. 11, no. 6, 2018.

[4] Y. Ren, L. Zhang, P. Shi, and Z. Zhang, "Research on multi-energy integrated ship energy management system based on hierarchical control collaborative optimization strategy," *Journal of Marine Science and Engineering*, vol. 10, no. 10, 2022.

[5] T.-T. Nguyen, B. L.-H. Nguyen, and T. Vu, "Energy management system for resilience-oriented operation of ship power systems," 2021.

[6] G. Rigatos, M. Hamida, M. Abbaszadeh, and P. Siano, "A nonlinear optimal control approach for shipboard ac/dc microgrids," *Electric Power Systems Research*, vol. 209, p. 108024, 2022. [Online]. Available: https://www.sciencedirect.com/science/article/pii/S0378779622002504

[7] E. Team, "Model description document notional four zone mvdc shipboard power system model," Electric Ship Research and Development Consortium, Tech. Rep., 2020.

[8] C. S. Greene, W. W. Weaver, D. G. Wilson, R. D. Robinett, R. C. Matthews, and S. Glover, "Reduced order model of a four-zone medium-voltage ac electric ship," in *2023 IEEE Electric Ship Technologies Symposium (ESTS)*, 2023, pp. 29–35.

[9] J. Young, D. G. Wilson, M. A. Cook, and W. Weaver, "Model predictive control for the operation of a hybrid mvac and mvdc electric warship," in *2023 IEEE Electric Ship Technologies Symposium (ESTS)*, 2023, pp. 317–326.

[10] J. T. Betts, *Practical Methods for Optimal Control and Estimation Using Nonlinear Programming*, 2nd ed. SIAM, 2010.

[11] C. de Boor and B. Swartz, "Collocation at gaussian points," *SIAM Journal on Numerical Analysis*, vol. 10, no. 4, pp. 582–606, 1973.

[12] J. A. Pietz, "Pseudospectral collocation methods for the direct transcription of optimal control problems," Master's thesis, Rice University, 2003.

[13] J. Young, D. G. Wilson, W. Weaver, and R. D. Robinett, "The optimal control with implicit phase coordination of a collective of wind turbines," in *21st Wind & Solar Integration Workshop (WIW 2022)*, vol. 2022, 2022, pp. 501–508.

[14] J. Young, D. G. Wilson, M. Cook, W. Weaver, M. A. Carbone, J. T. Csank, and J. Flicker, "Supervisory on-line optimal control of an electric power microgrid design for lunar habitation," in *AIAA SCITECH 2023 Forum*, 2023.

[15] J. Young, D. G. Wilson, R. D. R. III, and W. Weaver, "Supervisory optimal control with information flow for wind and solar resilient integration onto an electric power grid," *IET Conference Proceedings*, pp. 720–727(7), 2023.

[16] J. Young, D. G. Wilson, M. Cook, and W. Weaver, *Supervisory Optimal Control of an Electric Power Microgrid to Enhance In-Situ Resource Utilization for Lunar Habitats*.

[17] J. Young, D. G. Wilson, W. Weaver, and R. D. R. III, "A scalable optimal control algorithm for the operation of a resilient power grid architecture," Submitted, 2024.

[18] H. Prautzsch, W. Boehm, and M. Paluszny, *Bézier and B-Spline Techniques*. Springer, 2002.

[19] The MathWorks Inc., "Model predictive control toolbox," https://www.mathworks.com/products/model-predictive-control.html, 2022.

[20] M. A. Patterson and A. V. Rao, "Gpops-ii: A matlab software for solving multiple-phase optimal control problems using hp-adaptive gaussian quadrature collocation methods and sparse nonlinear programming," *ACM Trans. Math. Softw.*, vol. 41, no. 1, oct 2014. [Online]. Available: https://doi.org/10.1145/2558904

[21] J. D. Stevens, D. F. Opila, E. S. Oh, and E. L. Zivi, "All-electric warship load demand model for power and energy system analysis using exogenously initiated threats," in *2017 IEEE Electric Ship Technologies Symposium (ESTS)*, 2017, pp. 486–492.

[22] T. Hassell, W. W. Weaver, R. D. Robinett, D. G. Wilson, and G. G. Parker, "Modeling of inverter based ac microgrids for control development," in *2015 IEEE Conference on Control Applications (CCA)*, 2015, pp. 1347–1353.

[23] J. Young, "Optizelle – an open source software library designed to solve general purpose nonlinear optimization problems," www.optimojoe.com, 2013–2024.

[24] D. Ridzal, "Trust-region SQP methods with inexact linear system solves for large-scale optimization," PhD dissertation, Rice University, 2006.

[25] D. Ridzal, M. Aguiló, and M. Heinkenschloss, "Numerical study of matrix-free trust-region SQP method for equality constrained optimization," Sandia National Laboratories, Tech. Rep. SAND2011-9346, 2011.

[26] M. Heinkenschloss and D. Ridzal, "A matrix-free trust-region sqp method for equality constrained optimization," *SIAM Journal on Optimization*, vol. 24, no. 3, pp. 1507–1541, 2014.

[27] R. H. Byrd, M. E. Hribar, and J. Nocedal, "An interior point algorithm for large-scale nonlinear programming," *SIAM Journal on Optimization*, vol. 9, no. 4, pp. 877–900, 1999.

[28] T. A. Davis, "Algorithm 915, suitesparseqr: Multifrontal multithreaded rank-revealing sparse QR factorization," *ACM Trans. Math. Softw.*, vol. 38, no. 1, Dec. 2011.

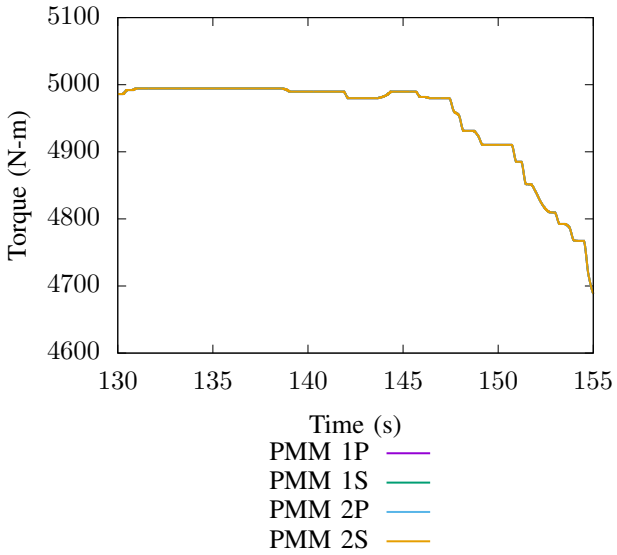

(a) Torque of the PMMs. For the PMMs, torque is specified parameter.

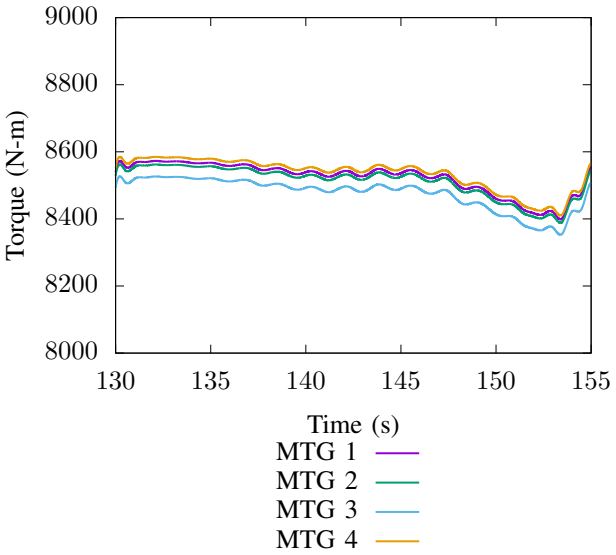

(b) Torque of the MTGs. For the MTGs, torque is a control input.

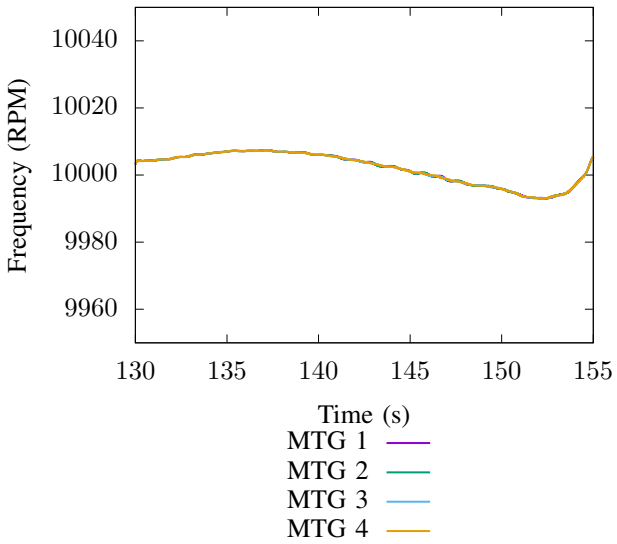

(c) Frequency of the MTGs. Note, less than 0.1% deviation in desired frequency

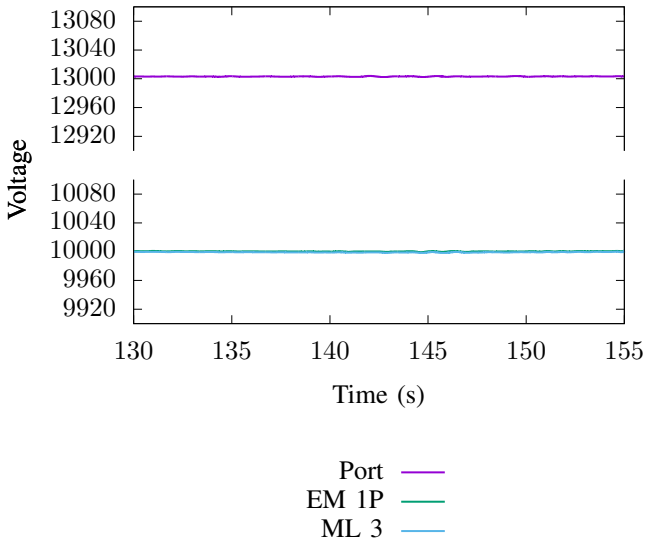

(d) Voltage on the parallel buses. Note, less than 0.1% deviation in desired voltage

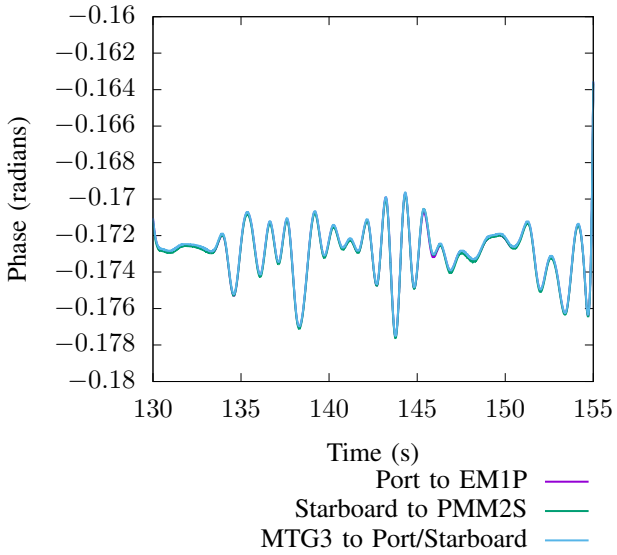

(e) Phase on the AC/DC transformers. Recall, this is a control input. Notice that most components sync their phase.

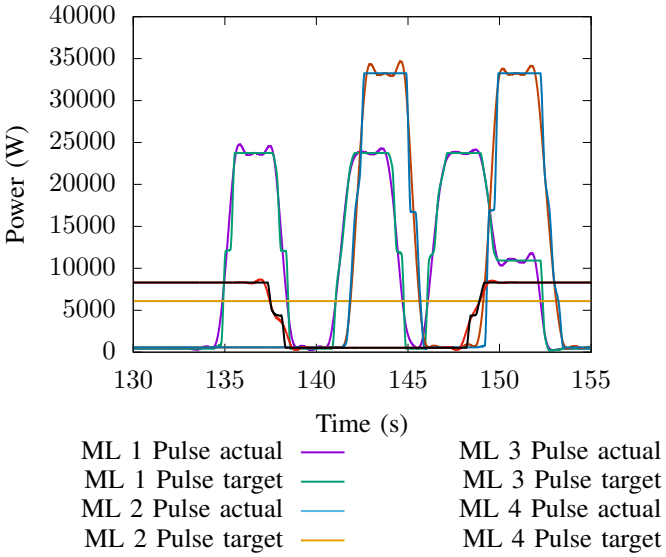

(f) Mission loads. Recall, this is a control input. It contains very minor ringing due to the step input in load.

Fig. 4: Performance of various the optimal control quantities for the electric ship